J Mater Sci: Mater Electron (2015) 26:2323–2328
DOI 10.1007/s10854-015-2687-y

Microstructure and electrical properties of $(Ba_{0.98}Ca_{0.02})(Ti_{0.94}Sn_{0.06})O_3$–*x* wt% ZnO lead-free piezoelectric ceramics sintered at lower temperature

Bo Wu · Dingquan Xiao · Jiagang Wu · Qian Gou · Jianguo Zhu

Received: 7 October 2014 / Accepted: 12 January 2015 / Published online: 18 January 2015

Abstract Lead-free piezoelectric ceramics of $(Ba_{0.98}Ca_{0.02})(Ti_{0.94}Sn_{0.06})O_3$–*x* wt% ZnO (BCTS–*x*ZnO) were synthesized by the conventional solid-state method. The microstructures and the electrical properties of BCTS–*x*ZnO ceramics were systematically studied in the composition range of $0 \leq x \leq 0.20$. It was found that the sintering temperature of BCTS ceramics was gradually decrease using ZnO as a sintering aid, and the addition of ZnO did not change the tetragonal phase structure of the ceramics. The BCTS–*x*ZnO ceramics with $x = 0.10$ sintered at a lower temperature of ~1,350 °C for 3 h demonstrated an optimum electrical behavior: $d_{33} \sim 428$ pC/N, $k_p \sim 53.3$ %, $2P_r \sim 24$ μC/cm^2, and $2E_c \sim 3.0$ kV/mm. As a result, the BCTS–*x*ZnO ceramic is a promising candidate for lead-free piezoelectric ceramics.

1 Introduction

Piezoceramics mainly based on lead zirconate titanate (PZT) ceramics at present certainly show great applications in microelectronic and micro-electromechanical devices due to their superior piezoelectric properties especially when the composition of the ceramics is close to the morphotropic phase boundary (MPB) between rhombohedral and tetragonal phases. Nevertheless, the ceramics are not environmental friendly because of the lead oxide toxicity. With the increase of worldwide concern, it is vital to develop replacement lead-free ceramics with comparable piezoelectric properties to those of PZT [1–4]. In the search for lead-free piezoelectric ceramics which have relatively good piezoelectric properties and high curie temperatures, considerable attention has been drawn for such as $(K_{0.50}Na_{0.50})NbO_3$ (KNN)- and $Bi_{0.50}Na_{0.50}TiO_3$ (BNT)-based ceramics [5–9]. However, the piezoelectric properties of the lead-free piezoelectric ceramics concerned are still lower than those of the $Pb(Zr,Ti)O_3$ (PZT) family ceramics. Therefore, it is urgent to find a new lead-free material system with higher piezoelectric properties to replace the lead-based ones.

Recently, researchers further revealed that the $BaTiO_3$ (BT) based ceramics, such as $Ba(Sn_{0.12}Ti_{0.88})O_3$–*x*$(Ba_{0.7}Ca_{0.3})O_3$ (BCTS), $Ba(Zr_{0.2}Ti_{0.8})O_3$–*x*$(Ba_{0.7}Ca_{0.3})TiO_3$ (BCTZ), have high piezoelectric coefficients of $d_{33} >$ 300–600 pC/N [10–14], i.e. the electrical properties of which ceramics are even higher than that of some lead-based ones. However, the ceramics with optimal composition and high d_{33} value were always sintered at a higher temperature of ≥1,450 °C. Therefore, it was expected that these ceramics could be fabricated through the lower temperature sintering, which not only will be good at suppressing the compositional change during ceramics sintering and reducing the energy consumption, but also reduces the processing costs especially in production. The studies published recently indicate that some reduce of the sintering temperature of the ceramics can be realized if a liquid-phase is formed during the sintering process through the sintering aid of doping oxides, and the sintering aid, such as CuO, MnO_2, CeO_2, Pr_2O_3, and HfO_2, is really an effective way to decrease the sintering temperature and improve the dense microstructure of the ceramics [14–22, 32]. However, there have been few systematical reports on the effect of ZnO used as a sintering aid on the microstructure and electrical properties of $Ba(Ti,Sn)O_3$–*x*$(Ba,Ca)TiO_3$ piezoelectric ceramics.

B. Wu · D. Xiao (✉) · J. Wu · Q. Gou · J. Zhu
Department of Materials Science, Sichuan University, Chengdu 610064, People's Republic of China
e-mail: nic0402@scu.edu.cn

In this work, the BCTS–xZnO ceramics were prepared by the conventional solid-state method, and all ceramics were sintered at 1,350 °C for 3 h. The effects of ZnO as a sintering aid on the phase structure, microstructure, dielectric and piezoelectric properties of BCTS ceramics were studied systematically.

2 Experimental procedure

$(Ba_{0.98}Ca_{0.02})(Ti_{0.94}Sn_{0.06})O_3$–$x$ wt% ZnO piezoelectric ceramics were prepared by the conventional solid-state reaction process. Raw materials of $BaCO_3$ (99.0 %), $CaCO_3$ (99.0 %), SnO_2 (99.0 %), TiO_2 (99.5 %) and ZnO (99 %) were mixed with ZrO_2 balls for 24 h by using the ethanol as a medium. After dried and calcined at 1,200 °C for 2 h, these powders were pressed into ~10 mm in diameter pellets and sintered at 1,350 °C for 3 h in air. Silver pastes were fired at ~700 °C for 10 min on both sides of these samples as electrodes for electrical measurements. All samples were poled at room temperature in a silicone oil bath under a *dc* field of ~4.0 kV/mm for 20 min.

The phase structure of these ceramics was measured by using X-ray diffraction (XRD) (Bruker D8 Advanced XRD, Bruker AXS Inc., Madison, WI, USA). Scanning electron microscopy (SEM, Philips, XL30) was employed to study the surface morphologies of these ceramics. The dielectric behavior as a function of the measurement temperature of these ceramics was measured by using an LCR meter (HP 4980, Agilent, USA), and their piezoelectric constant d_{33} of the ceramics was measured by using a piezo-d_{33} meter (ZJ-3A, China). The polarization versus electric field (P–E) hysteresis loops of the ceramics was measured by using a Radiant Precision Workstation (USA).

3 Results and discussion

Figure 1a plots the room temperature XRD patterns of ZnO-doped BCTS ceramics with different x contents. It is evident that the ceramics show pure perovskite phase and no secondary phases can be certified in the investigated θ range of XRD. That is, the dopant has completely diffused into the BCTS lattice to form a homogeneous solid solution. As shown from Fig. 1b, the enlarged diffraction patterns at around 45° show that the diffraction peaks of all ceramics split into (002) and (200) double peaks, which well matches the PDF card of tetragonal $BaTiO_3$ (PDF#05-0626). This result indicates that the ZnO-doped BCTS ceramics possess a tetragonal phase at room temperature. As a result, the addition of ZnO did not change the phase structure of BCTS ceramics. Moreover, compared with that of the pure BCTS ceramics, the XRD peaks of ZnO-doped BCTS ceramics shifted to a low angle with an increase in ZnO content when $x \leq 0.10$, then it shifted to a high angle when x further increases to 0.20. Undoubtedly, the introduction of Zn is the reason for the shift of diffractions peaks. As we known, the ionic radius of Zn^{2+} (0.74 Å) is much smaller than those of A-site ions (Ba^{2+}: 1.61 Å, Ca^{2+}: 1.35 Å), while the radius of Zn^{2+} is close those of Ti^{4+} (0.61 Å) and Sn^{4+} (0.71 Å). Therefore, the Zn ions are more likely to substitute the B site of BCTS, which would lead to the increase of lattice parameter. And the above fact can qualitatively explain the shift of diffraction peaks towards lower angle when $x \leq 0.10$. In addition, the underlying physical mechanisms of the abnormal phenomenon when $x > 0.10$ have been reasonably explained by two aspects. Firstly, owing to the limit of solid solubility of Zn^{2+} ions in the BCTS matrix, the excessive Zn^{2+} ions stockpile in the grain boundaries and suppress the grain growths. Secondly, it was reported that the oxygen vacancies can be induced by the substitutions for a higher valence B site using a lower valence [23]. This is, oxygen vacancies ($ZnO = Zn_{(Ti,Sn)}'' + V_O.. + O_O$) are generated when the Zn substitutes for the (Ti, Sn) site. The generation of oxygen vacancies resulted in a distortion and contraction of unit cells from the viewpoint of crystal chemistry [24]. In this work, the shift of the diffraction peaks is caused by two distinct effects: the ion radius effect seems to be the main contributing factor at relatively low Zn content, while the oxygen vacancy effect appears to be the main one at relatively high Zn content.

To further confirm the phase structure of the ceramics, their Raman spectra was measured in the region of 100–1,000 cm^{-1}, as shown in Fig. 2. The longitudinal (LO) and transverse (TO) components are split due to the long electrostatic force associated with the lattice iconicity induced by Ba^{2+} ions in BCTS [25]. The Raman modes of $BaTiO_3$-based materials are assigned to be $E(TO_1)$, $A_1(TO_1)$, $A_1(TO_2)$, $E(TO_2)$, $A_1(TO_3)$ and $A_1(LO_3)/E(LO_3)$ in the range of 150–1,000 cm^{-1}. The tetragonal structure of $BaTiO_3$-based materials could be confirmed by the $E(TO_2)$ phonon mode [26]. Therefore, the micro-Raman scattering spectra and the XRD pattern also conforms the tetragonal phase structure in BCTS ceramics.

To clearly study the ZnO effect on the surface morphologies of BCTS ceramics, the SEM patterns are shown in Fig. 3a–d. It is observed that the microstructure of ZnO-doped BCTS ceramics is strongly dependent on the introduction of ZnO. When the ZnO was doped ($x \leq 0.1$ wt%), the grain size of the ceramics had a homogeneous microstructure. Moreover, small amounts of liquid phases were formed with increasing x (0.03–0.10), resulting in a denser microstructure of BCTS ceramics in this work. The fact that the lower valence states of Zn^{2+} substitute the higher

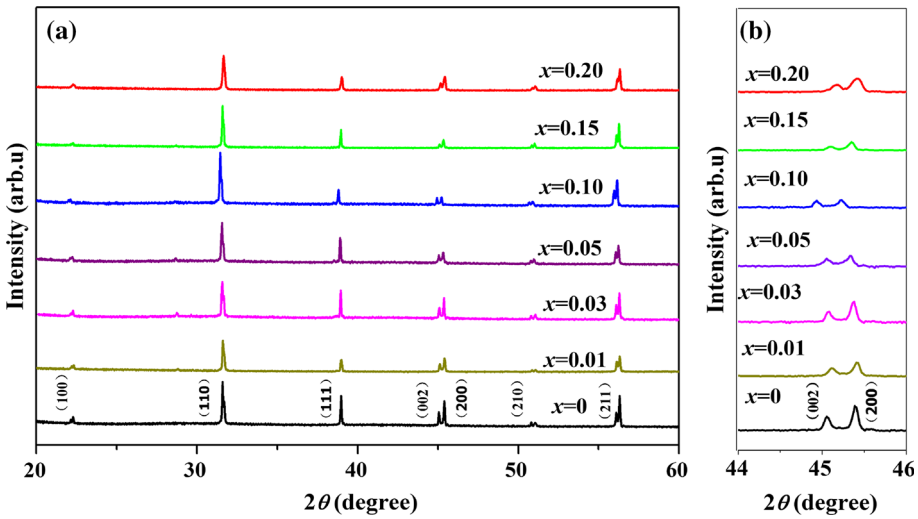

Fig. 1 **a** XRD patterns and **b** expanded XRD patterns in the 2θ range of 44°–46° of ZnO-doped BCTS ceramics

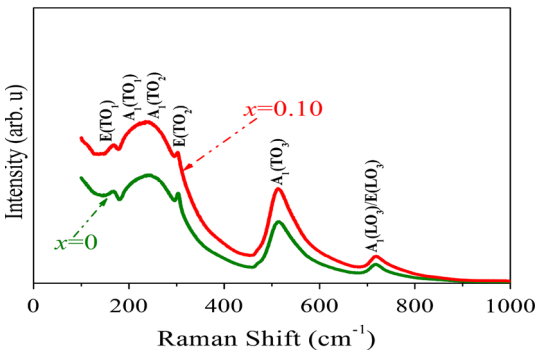

Fig. 2 Raman spectroscopy of ZnO-doped BCTS ceramics

valence states of Ti^{4+}/Sn^{4+} generates oxygen vacancies, which enhances the transfer of mass and energy among reactions resulting the improvement of the sintering behavior [27–29]. With further addition of Zn content ($x > 0.1$ wt%), the grain growths are restrained, and some pores appear. The underlying physical mechanisms have been reasonably explained below: a low ZnO content promotes the grain growths of BCTS ceramics by entering the lattice, while the excess ZnO content may stockpile in the grain boundaries and suppress the grain growths.

Figures 4a, b plot the temperature dependence of the dielectric constant (ε_r) and the dielectric loss (tan δ) of ZnO-doped BCTS ceramics respectively in the temperature

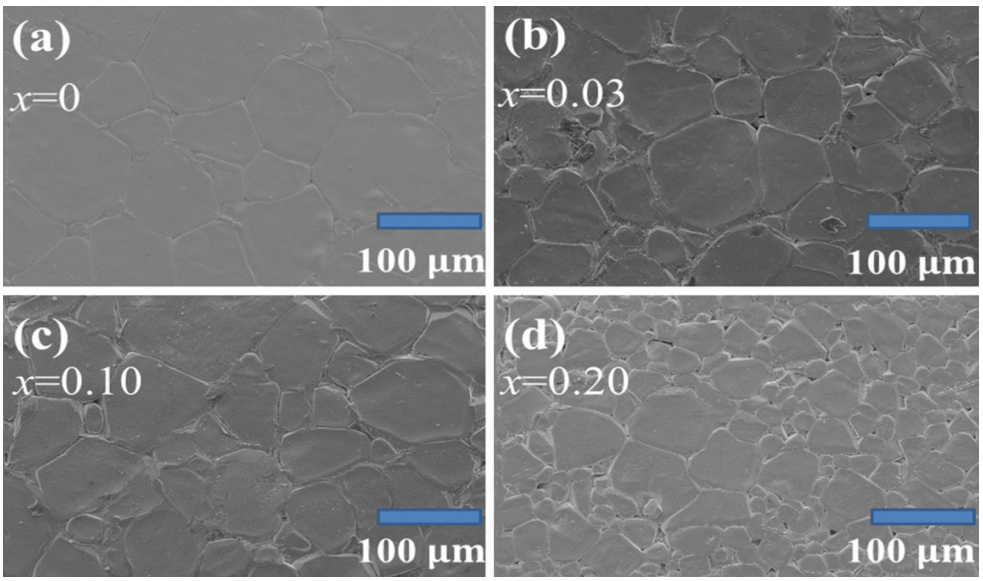

Fig. 3 SEM surface micrographs of ZnO-doped BCTS ceramics, **a** $x = 0$, **b** $x = 0.03$, **c** $x = 0.10$, and **d** $x = 0.20$

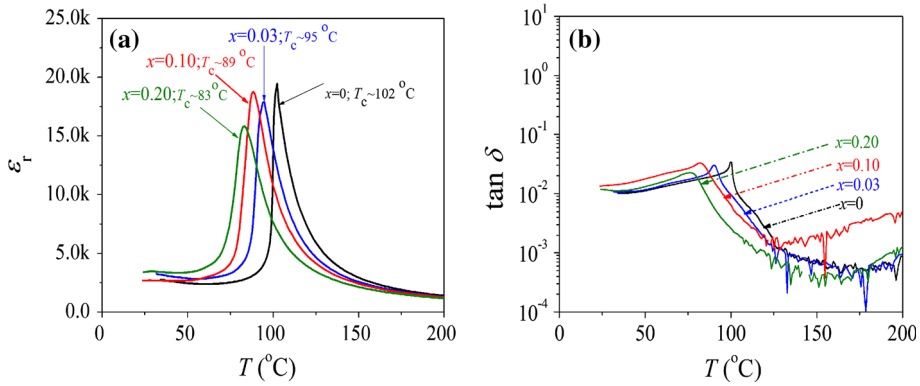

Fig. 4 Temperature dependence of **a** dielectric constant and **b** dielectric loss of ZnO–doped BCTS ceramics

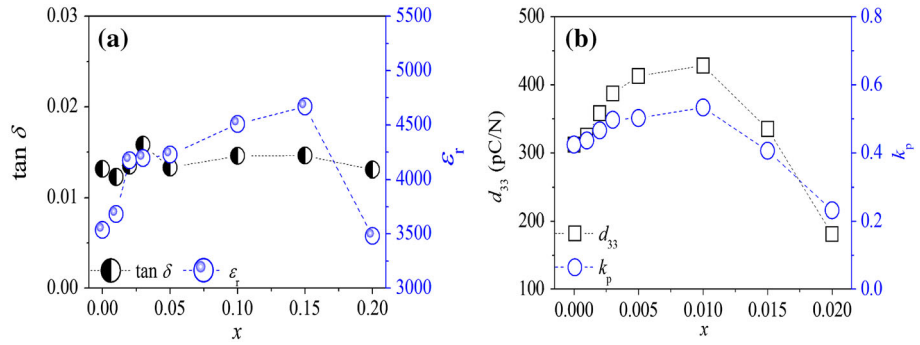

Fig. 5 **a** Dielectric and **b** piezoelectric properties of ZnO-doped BCTS ceramics

range of room temperature to 200 °C at 10 kHz. It is observed from Fig. 3a that the tetragonal–cubic phase transition (T_C) temperature of ZnO-doped BCTS ceramics decreases slightly with increasing ZnO content. The decrease in T_C reflects the incorporation of Zn^{2+} into the BCTS lattice, and the amount of ZnO incorporated as solid solution also increases with increasing ZnO content, a similar result has been shown elsewhere [14, 33]. Moreover, a lower dielectric loss (tan $\delta < 1.6$ %) is demonstrated in ZnO-doped BCTS ceramics, as shown in Fig. 4b.

Figure 5a plots the ε_r and tan δ values of BCTS ceramics as a function of ZnO content, measured at room temperature of ~20 °C. It was observed that the ε_r values of ZnO-doped BCTS ceramics obviously increase in the compositional range of $x \leq 0.15$, getting a lager value (4,500–4,800) at $0.10 \leq x \leq 0.15$, and then decrease with further rising ZnO content ($x > 0.15$) because of a lower density as well as the formation of some pores, as shown in Fig. 2d. Moreover, the ZnO-modified BCTS ceramics have a low tan δ value (0.012–0.016) regardless of ZnO contents. Figure 5b plots the piezoelectric behavior of ZnO-doped BCTS ceramics, measured at room temperature. The d_{33} value increases with increasing ZnO content, reaching a maximum value of $d_{33} \sim 428$ pC/N at the dopant of $x = 0.10$, and then sharply drops with further increasing the dopant. Similar to the change of the d_{33} value, the k_P value of the ZnO-doped BCTS ceramics also reaches a

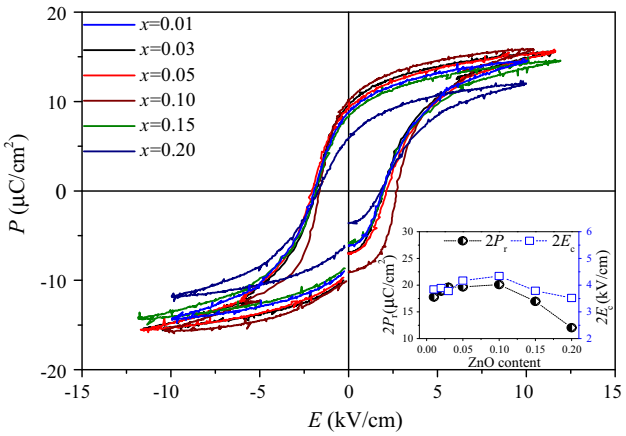

Fig. 6 *P–E* loops of ZnO-doped BCTS ceramics, and the insert shows the $2P_r$ and $2E_c$ values of ZnO-doped BCTS ceramics

maximum value of ~53.3 % at $x = 0.10$. In this work, the improvement of the piezoelectric properties is fundamentally caused by two aspects. Firstly, the improved piezoelectric property of the ceramics is partly attributed to the dense and homogeneous microstructure of the optimized BCTS–0.1ZnO ceramics, which is benefited from the liquid sintering due to the introduction of Zn sintering aids, as shown in Fig. 3c. Secondly, the piezoelectric properties are also related to the dielectric and ferroelectric properties of ferroelectric materials, that is, $d_{33} \sim \alpha\varepsilon_r P_r$ [34, 35]. In this

Table 1 Piezoelectric properties and sintering temperature of BCTS-based ceramics

Materials system	d_{33}/(pC/N)	k_p	T_s/(°C)	Refs.
$Ba(Sn_{0.12}Ti_{0.88})O_3$–$x(Ba_{0.7}Ca_{0.3})O_3$	530	–	1,450	[11]
$(Ba_{1-x}Ca_x)(Ti_{0.95}Sn_{0.05})O_3$	464	43.1 %	1,450	[30]
$(1-x)Ba_{0.98}Ca_{0.02}Ti_{0.94}Sn_{0.06}O_3$–$xBa_{0.85}Ca_{0.15}Ti_{0.9}Zr_{0.1}O_3$	407	28 %	1,380	[31]
$(Ba_{0.98}Ca_{0.02})(Ti_{0.94}Sn_{0.06})O_3$–$x$mol%$HfO_2$	430	48 %	1,400	[22]
$(Ba_{0.98}Ca_{0.02})(Ti_{0.94}Sn_{0.06})O_3$–$x$mol%CuO	367	48.7 %	1,300	[32]
$(Ba_{0.98}Ca_{0.02})(Ti_{0.94}Sn_{0.06})O_3$–$x$wt%ZnO	428	53.3 %	1,350	This work

work, the ZnO-doped BCTS ceramic with $x = 0.10$ has a higher ε_r value and a larger P_r value, as shown in Figs. 5a and 6, so the d_{33} and $\varepsilon_r P_r$ simultaneously reach maximum for the ceramic with $x = 0.1$, confirming that enhanced dielectric and ferroelectric properties should be partly responsible for its enhanced piezoelectricity. As a result, the improvement in d_{33} value could be attributed to the enhancement of the dielectric properties, ferroelectric properties and dense microstructure of ZnO-doped BCTS ceramic.

Table 1 gives the piezoelectric properties and the sintering temperature of BCTS-based ceramics published in the literature recently. From Table 1 one can clearly see that till now, there were few reports on relatively high piezoelectric properties ($d_{33} \sim 428$ pC/N and $k_p \sim 53.3$ %) of BCTS ceramics when sintered at such a low temperature of ~1,350 °C as in present work.

Figure 6 shows the P–E loops of ZnO-doped BCTS ceramics with different ZnO contents measured at 10 Hz and room temperature of ~20 °C. It is observed from Fig. 6 that all the loops are saturated and have a typical ferroelectric behavior. The insert of Fig. 6 shows the $2P_r$ and $2E_c$ values of ZnO-doped BCTS ceramics, the remnant polarization (P_r) of ZnO-doped BCTS ceramics slightly increases in the compositional range of $x \leq 0.10$, reaches a maximum value of ~24 μC/cm^2 at the doping content of $x = 0.10$, and then decreases with further rising ZnO content. In addition, the change of E_c value is similar as compared with the P_r, the $2E_c$ is in the range of 3.0–4.2 kV/cm.

4 Conclusions

$(Ba_{0.98}Ca_{0.02})(Ti_{0.94}Sn_{0.06})O_3$–$x$ wt% ZnO (BCTS–xZnO) lead-free piezoelectric ceramics were prepared by the conventional solid-state method with a lower sintering temperature of ~1,350 °C. The ceramics with $x = 0.10$ shows an excellent high piezoelectric performance of $d_{33} \sim 428$ pC/N, $k_p \sim 53.3$ %, $2P_r \sim 24$ μC/cm^2, and $2E_c \sim 3.0$ kV/mm. Experimental results indicate that the addition of ZnO as a sintering aid plays an important role in the microstructure, dielectric and piezoelectric properties of BCTS ceramics with a relatively lower sintered temperature, which shows that the ceramics possess a promising future for lead-free piezoelectric devices.

Acknowledgments Authors gratefully acknowledge the supports of the National Science Foundation of China (NSFC Nos. 50772068, 50972095, 51102173, 51272164, and 51332003), the Fundamental Research Funds for the Central Universities, and the introduction of talent start funds of Sichuan University (2082204144033). And the authors also thank Ms. Wang Hui for her help in the SEM measurement.

References

1. Y. Saito, H. Takao, T. Tani, T. Nonoyama, K. Takatori, T. Homma, Nature **432**, 84 (2004)
2. J. Rödel, W. Jo, K.T.P. Seifert, M. Anton, T. Granzow, D. Damjanovic, J. Am. Ceram. Soc. **92**, 1153 (2009)
3. D.Q. Xiao, J.G. Wu, L. Wu, J.G. Zhu, P. Yu, D.M. Lin, Y.W. Liao, Y. Sun, J. Mater. Sci. **44**, 5408 (2009)
4. L.E. Cross, Nature **432**, 24 (2004)
5. J.F. Li, K. Wang, F.Y. Zhu, L.Q. Cheng, F.Z. Yao, J. Am. Ceram. Soc. **96**, 3677 (2013)
6. D.M. Lin, D.Q. Xiao, J.G. Zhu, P. Yu, Appl. Phys. Lett. **88**, 062901 (2006)
7. H. Nagata, M. Yoshida, Y. Makiuchi, T. Takenaka, Jpn. J. Appl. Phys. **42**, 7401 (2003)
8. J.G. Wu, D.Q. Xiao, Y.Y. Wang, J.G. Zhu, L. Wu, Y.H. Jiang, Appl. Phys. Lett. **91**, 252907 (2007)
9. D. Lin, D.Q. Xiao, J.G. Zhu, P. Yu, H.J. Yan, L.Z. Li, Mater. Lett. **58**, 615–618 (2004)
10. W.F. Liu, X.B. Ren, Phys. Rev. Lett **103**, 257602 (2009)
11. D.Z. Xue, Y.M. Zhou, H.X. Bao, J.H. Gao, C. Zhou, X.B. Ren, Appl. Phys. Lett. **99**, 122901 (2011)
12. S.W. Zhang, H.L. Zhang, B.P. Zhang, S. Yang, J. Alloy. Compd. **506**, 131 (2010)
13. J.G. Wu, D.Q. Xiao, W.J. Wu, J.G. Zhu, J. Wang, J. Alloys, Compd. **509**, L359 (2011)
14. J.G. Wu, D.Q. Xiao, W.J. Wu, Q. Chen, J.G. Zhu, Z. Yang, J. Wang, Script. Mater. **65**, 771 (2011)
15. I. Burn, US patent 4283753, 1981
16. C.F. Yang, L. Wu, T.S. Wu, J. Mat. Sci. **27**, 6573 (1992)
17. P. Zheng, J.L. Zhang, S.F. Shao, Y.Q. Tan, C.L. Wang, Appl. Phys. Lett. **94**, 032902 (2009)
18. C.C. Tsai, S.Y. Chu, C.H. Lu, IEEE Trans. Ultrason. Ferroelectr. Freq. Control **56**, 660 (2009)
19. Y.C. Lee, Y.L. Huang, J. Am. Ceram. Soc. **92**, 2661 (2009)
20. S. Derling, Th Müller, H.-P. Abicht, K.-H. Felgner, H.T. Langhammer, J. Mater. Sci. **36**, 1425 (2001)
21. A. Ramesh Babu, A.V. Prasadarao, J. Mater. Sci. Lett. **16**, 313 (1997)

22. J.G. Wu, T. Wang, X.J. Cheng, X.P. Wang, B.Y. Zhang, J.G. Zhu, D.Q. Xiao, J. Alloys Compd. **576**, 299 (2013)
23. H.C. Hu, M.K. Zhu, F.Y. Xie, N. Lei, J. Chen, Y.D. Hou, H. Yan, J. Am. Ceram. Soc. **92**, 2039 (2009)
24. Q. Xu, M. Chen, W. Chen, H.X. Liu, B.H. Kim, B.K. Ahn, Acta Mater. **56**, 642 (2008)
25. P.S. Dobal, R.S. Katiyar, J. Raman Spectrosc. **33**, 405 (2002)
26. B.D. Begg, K.S. Finnie, E.R. Vance, J. Am. Ceram. Soc. **79**, 2666 (1996)
27. T. Chen, T. Zhang, G.C. Wang, J.F. Zhou, J.W. Zhang, Y.H. Liu, J. Mater. Sci. **47**, 4612 (2012)
28. M.K. Zhu, L.Y. Liu, Y.D. Hou, H. Wang, H. Yan, J. Am. Ceram. Soc. **90**, 120 (2007)
29. A. Watcharapasorn, S. Jiansirisomboon, Ceram. Int. **34**, 769 (2008)
30. M.L. Chen, Z.J. Xu, R.Q. Chu, H. Qiu, M. Li, Y. Liu, L. Shao, S. Ma, W.B. Ji, W. Li, S.W. Gong, G.R. Li, Phys. B **433**, 43 (2014)
31. J.G. Wu, A. Habibul, X.J. Cheng, X.P. Wang, B.Y. Zhang, Mater. Res. Bull. **48**, 4411 (2013)
32. B. Wu, D.Q. Xiao, J.G. Wu, T. Huang, Z. Wang, C. Liu, F.X. Li, J.G. Zhu, J. Electroceram. (2014). doi:10.1007/s10832-014-9949-6
33. A.C. Caballero, J.F. Fernandez, C. Moure, P. Duran, J. Eur. Ceram. Soc. **17**, 513 (1997)
34. X.P. Wang, J.G. Wu, D.Q. Xiao, X.J. Cheng, T. Zheng, B.Y. Zhang, X.J. Lou, J.G. Zhu, J. Mater. Chem. A **2**, 4122 (2014)
35. X.P. Wang, J.G. Wu, X.J. Cheng, B.Y. Zhang, D.Q. Xiao, J.G. Zhu, X.J. Wang, X.J. Lou, J. Phys. D Appl. Phys. **46**, 495305 (2013)